Petroleum Science
https://doi.org/10.1007/s12182-020-00512-3

ORIGINAL PAPER

3D anatomy and flow dynamics of net-depositional cyclic steps on the world's largest submarine fan: a joint 3D seismic and numerical approach

Da-Li Shao[1] · Guo-Zhang Fan[1] · Hai-Qiang Wang[2] · Hong-Xia Ma[1] · Guo-Ping Zuo[1] · Liang-Bo Ding[1] · Zheng Cai[2] · Wei-Qiang Li[1]

Received: 20 January 2020

Abstract
Supercritical flows are ubiquitous in natural environments; however, there is rare 3D anatomy of their deposits. This study uses high-quality 3D seismic datasets from the world's largest submarine fan, Bengal Fan, to interpret 3D architectures and flow processes of Pliocene undulating bedforms that were related to supercritical flows. Bengal undulating bedforms as documented in this study were developed in unconfined settings, and are seismically imaged as strike-elongated, crescentic bedforms in plan view and as rhythmically undulating, upstream migrating, erosive, discontinuous reflections in section view. Their lee sides are overall 3 to 4 times steeper (0.28° to 1.19° in slope) and 3 to 4 times shorter (117 to 419 m in length) than their stoss flanks and were ascribed to faster (high flow velocities of 2.70 to 3.98 m/s) supercritical flows (Froude numbers of 1.53 to 2.27). Their stoss sides, in contrast, are overall 3 to 4 times gentler (0.12° to 0.27° in slope) and 3 to 4 times longer (410 to 1139 m in length) than their lee flanks and were related to slower (low velocities of 2.35 to 3.05 m/s) subcritical flows (Froude numbers of 0.58 to 0.97). Bengal wave-like features were, thus, created by supercritical-to-subcritical flow transformations through internal hydraulic jumps (i.e., cyclic steps). They have crests that are positive relative to the surrounding region of the seafloor, suggesting the predominant deposition of draping sediments associated with net-depositional cyclic steps. Turbidity currents forming Bengal wave-like features were, thus, dominated by deposition, resulting in net-depositional cyclic steps. Sandy deposits associated with Bengal net-depositional cyclic steps are imaged themselves as closely spaced, strike-elongated high RMS-attribute patches, thereby showing closely spaced, long and linear, strike-elongated distribution patterns.

Keywords Sediment waves · Net-depositional cyclic steps · Supercritical flows · Sandy supercritical-flow deposits · Bengal Fan

1 Introduction

The importance of the supercriticality of turbidity currents has long been acknowledged, when turbidity currents travel on a slope with gradients of $> 0.6°$ (e.g., Komar 1971; Hand 1974). Recent physical and numerical models have shown that supercritical-flow regimes are fairly common on Earth (e.g., Sun and Parker 2005; Kostic et al. 2010; Cartigny et al. 2011, 2014). Froude-supercritical turbidity currents traveling through erodible sediment beds may give rise to cyclic steps and related supercritical bedforms, such as antidunes, chutes-and-pools, and sediment waves (e.g., Fildani et al. 2006; Kostic 2011; Cartigny et al. 2014; Covault et al. 2014, 2017; Vellinga et al. 2018). In the light of recent theoretical and experimental progresses in supercritical flows (e.g., Fildani et al. 2006; Cartigny et al. 2014; Hughes Clarke et al. 2014; Hughes Clarke 2016; Vellinga et al. 2018), cyclic steps and related supercritical bedforms have only recently been recognized in the natural environments (e.g., Fildani et al. 2006; Kostic 2011; Cartigny et al. 2014; Covault

Edited by Jie Hao

✉ Hong-Xia Ma
mahx_hz@petrochina.com.cn

[1] PetroChina Hangzhou Research Institute of Geology, Hangzhou 310023, Zhejiang, China

[2] Chinnery Assets Limited, Yangon, Myanmar

Published online: 19 November 2020

et al. 2014, 2017; Postma and Cartigny 2014; Ventra et al. 2015; Hughes Clarke 2016; Gong et al. 2017; Li and Gong 2018). They are increasingly acknowledged as the main building blocks and constituents of deep-water depositional systems, forming some so-called supercritical submarine fans (sensu Paul et al. 2017) (e.g., Pickering et al. 2015; Symons et al. 2016; Covault et al. 2014, 2017; Lang et al. 2017). They have been observed in a large number of depositional settings, including fluvio-deltaic systems (Hughes Clarke et al. 2014; Ventra et al. 2015; Dietrich et al. 2016; Hughes Clarke 2016), submarine canyons (e.g., Heiniö and Davies 2009; Paull et al. 2010; Covault et al. 2014; Zhong et al. 2015), subaqueous fans (e.g., Pickering et al. 2015), glacial outwash plains (e.g., Lang and Winsemann 2013), overbank areas (e.g., Fildani et al. 2006; Armitage et al. 2012), and the modern submarine seafloor (Symons et al. 2016).

Cyclic steps (i.e., long-wave, upstream-migrating, upper-flow-regime bedforms bounded by transitions from densimetric Froude supercritical-to-subcritical flows) can be generally classified into three main categories (i.e., net-erosional, transportational, and net-depositional cyclic steps), depending on whether the dominant processes across the bedforms are erosional or depositional (Fildani et al. 2006; Cartigny et al. 2011; Kostic 2011; Covault et al. 2014, 2017; Zhong et al. 2015). Net-erosional cyclic steps are manifested as trains of upstream-migrating scours, whereas net-depositional cyclic steps take the form of upstream-migrating sediment waves (e.g., Fildani et al. 2006; Lamb et al. 2008; Kostic 2011; Covault et al. 2014, 2017; Symons et al. 2016). Transportational cyclic steps, which are neither net-erosive nor net-depositional (Parker and Izumi 2000), have been experimentally observed in flume tanks (Taki and Parker 2005; Cartigny et al. 2014) and computational fluid-dynamics models (Vellinga et al. 2018). They appear in the depth-resolved numerical model of Vellinga et al. (2018) as an amalgamation of concave-up erosion surfaces and preserved low-angle backsets and foresets. In addition, the most recent work of Slootman and Cartigny (2019) has promoted another classification scheme; based on the ration between the rates of bed aggradation and bedform migration, four main types of cyclic steps are fully depositional, partially depositional, partially erosional, and fully erosional. In spite of the recent furry of the recognition of supercritical bedforms, the topic of supercritical-flow regimes has yielded significant debate at the international workshop of Talling et al. (2015). Such ongoing debate is partly ascribed to a shortage of 3D anatomy of upper-flow-regime bedforms (Cartigny et al. 2014; Kostic 2014; Vellinga et al. 2018), with the notable exception of Heiniö and Davies 2009. Therefore, it is now time to go back to some major turbidite systems to better understand what features are (or are not) created by supercritical flows and their 3D architectures (Talling, et al. 2015).

Large-scale, undulating sediment waves are known as the most widespread, and frequently described net-depositional cyclic steps in deep-water settings (e.g., Fildani et al. 2006; Lamb et al. 2008; Covault et al. 2017; Symons et al. 2016). Normark et al. (2002) have suggested that sediment waves contain sandy deposits, which may form important repositories for subsurface oil and gas reservoirs worldwide, with considerable economic and strategic significance. However, the exploration significance of sandy supercritical-flow deposits remains elusive. The occurrence of previously undocumented, seismically undulating bedforms of Pliocene age on the Bengal Fan (Figs. 1, 2), together with 2000 km^2 high-quality (15 to 20 m vertical and 12.5 m lateral resolution), time-migrated 3D seismic database, provides an excellent opportunity to: (i) investigate 3D seismic stratigraphy and geomorphology of net-depositional cyclic steps (i.e., sediment waves); (ii) estimate parameters of turbidity currents forming Bengal undulatory bedforms; and (iii) identify where thick sand beds that might be important as hydrocarbon reservoirs can be found in the studied cyclic steps.

2 Geological settings and the study area

The study area of the present study (hot color-shaded box in Fig. 1) is located in the Rakhine Basin, with a water depth of 1300 to 2100 m. Rakhine Basin is a Tertiary foredeep basin located in the eastern fringe of the Bay of Bengal and western coastal provinces of Myanmar that is floored by the Bengal Fan (Fig. 1; Curray 2014; Yang and Kim 2014). It is predominantly an offshore basin, with the onshore parts comprising low lying islands and coastal areas. The evolution of the Rakhine Basin is closely related to the northeastward oblique subduction of the Indian plate beneath Burmese microplates since the Paleocene and the ensuing westward migration of the developing accretionary wedge. Thus, the associated compressional tectonic forces have decreased to the offshore area, and accordingly, the deformation intensity of the strata shows a decreasing trend from east to west.

The Bengal Fan is approximately 3000 km long, with a maximum thickness of up to 16.5 km (Fig. 1; Curray 2014; Yang and Kim 2014). It varies in width from 830 to 1430 km and occupies an area of approximately 3×10^6 km^2 (Fig. 1; Curray 2014). The development of the Bengal Fan was initiated by the uplift of the Himalayas due to the collision between India and Asia in the Early Eocene (Yin 2006; Bastia et al. 2010). It underwent two main stages of tectonic-stratigraphic evolution thereafter, namely an initial rifting stage from early Eocene to middle Miocene and a postrifting stage from late Miocene to Holocene (Bastia et al. 2010). These two tectonic-stratigraphic subdivisions are bounded at their base by two basin-wide unconformities dated at early Eocene and late

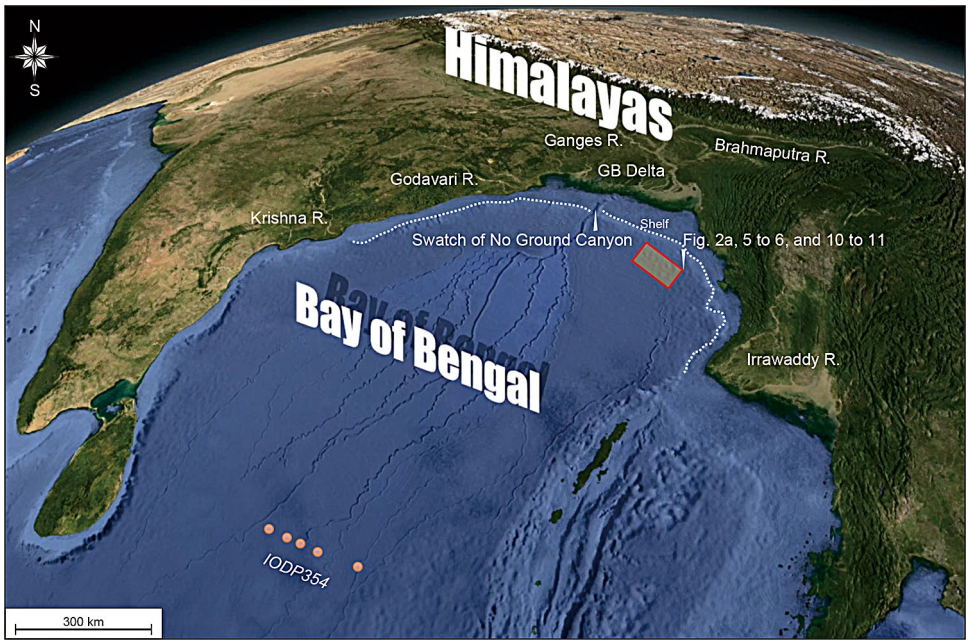

Fig. 1 Physiography map of Ganges–Brahmaputra source-to-sink system. Note that the study area (hot color-shaded box) is located in the Rakhine Basin, northeastern Bengal Fan. Also shown are regional plan-view locations of geomorphic images presented in Figs. 2a, 5, 6, 10, and 11. Ganges R. = Ganges River, Brahmaputra R. = Brahmaputra River, GB Delta = Ganges–Brahmaputra delta, Godavari R. = Godavari River, Krishna R. = Krishna River, and Irrawaddy R. = Irrawaddy River

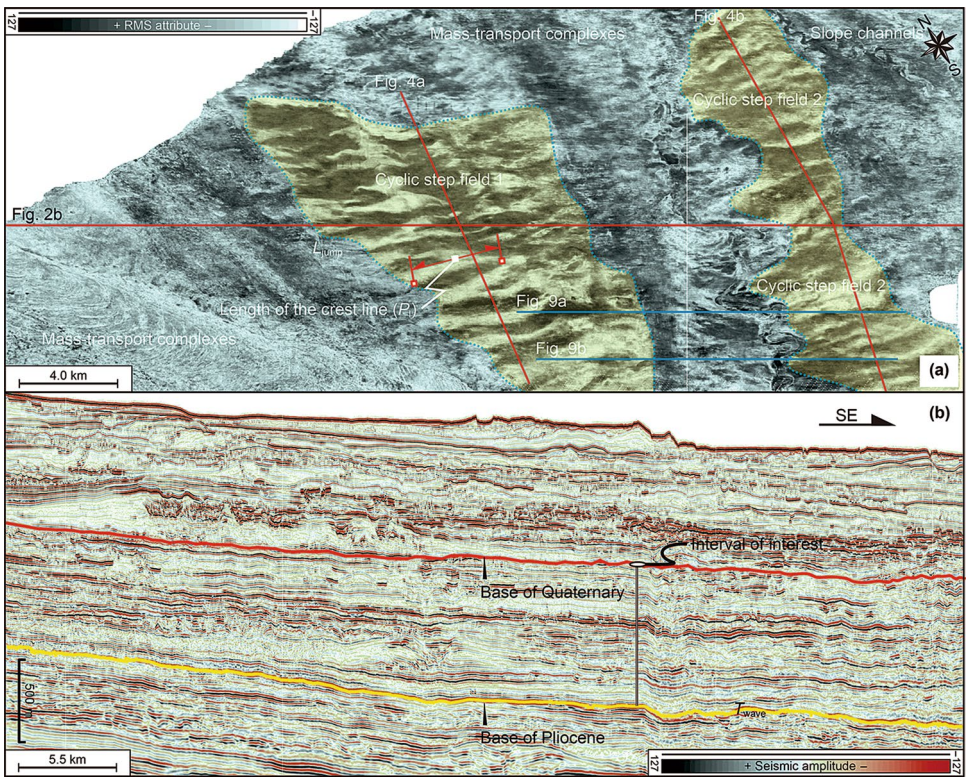

Fig. 2 Bengal wave-like features appeared on RMS attribute-extraction map and strike-view seismic profile (upper and lower panels, respectively). Also shown are plan-view locations of seismic sections presented in Figs. 2b, 4a, b, and 9a, b and stratigraphic positions of the hanging horizon of T_{wave}. Note that Pliocene Bengal turbidite systems are our study interval of interest

Miocene, respectively (Krishna et al. 2009; Yang and Kim 2014). The early Eocene unconformity is recognized as the Paleocene-Eocene hiatus and marks the initiation of the India collision, Himalayan uplift, and the Bengal Fan sedimentation (Curray et al. 2003; Krishna et al. 2009). The late Miocene unconformity records the intraplate deformation of the oceanic lithosphere created by the collision of India and Asia (Krishna et al. 2009; Yang and Kim 2014).

The Himalayan-sourced Ganges–Brahmaputra river system and concomitant Bengal Fan represents the Earth's largest present-day source-to-sink system (Blum et al. 2018). Driven by the early Eocene to the recent tectonic uplift of the Himalayas induced by the collision of India and Asia, sediments eroded from the Himalayas have shed into the Bengal basin and the Bay of Bengal through the Ganges–Brahmaputra rivers with a sediment load of ca 1.2×10^9 t/yr (Fig. 1; Curray 2014). The delivery of sediment from Ganges–Brahmaputra deltas (the largest deltaic system on Earth) into the Bay of Bengal was achieved mainly through the 'Swatch of No Ground' (Fig. 1; Blum et al. 2018), which landward disappears in a water depth of 38 m, and seaward continues for nearly 160 km, to a water depth of at least 1400 m (Bastia et al. 2010). Swatch of No Ground acts as a temporary trap for sediments dispersal from Ganges–Brahmaputra river-delta systems by storms and/or tides on the shelf (e.g., Curray et al. 2003; Michels et al. 2003; Schwenk et al. 2005). Sediments within the Swatch of No Ground were further remobilized, and were then transported to the outlying deep-water areas by turbidity currents (e.g., Curray et al. 2003; Kottke et al. 2003; Michels et al. 2003; Schwenk et al. 2005). Such sediment-routing processes, in turn, fostered the volumetrically most significant turbidity currents and resultant turbidite systems (Fig. 2a, b), which have remained active even during Holocene highstand (Weber et al. 1997; Fournier et al. 2016).

Turbidite systems in Rakhine Basin have received considerable attention recently, due to the discovery of the commercial Shwe gas field in the Rakhine turbidite systems of Pliocene age (e.g., Yang and Kim 2014; Zhan et al. 2019; Ma et al. 2020). The recoverable gas reserves from the Shwe gas field were estimated to contain 4 trillion cubic feet of extremely dry gas (Yang and Kim 2014). Pliocene turbidite systems in Rakhine Basin, northeastern Bengal Fan fostered a series of seismically well-imaged undulating bedforms whose 3D architectures and flow dynamics are the focus of the current study (Fig. 2b).

3 Database and methodology

The primary data utilized in this study are 2000 km^2 of commercial 3D seismic-reflection data shoot by I/O sleeve air gun. They have a 4 ms vertical sampling rate and a bin spacing of 25 m (inline) × 12.5 m (crossline). 3D seismic data have been processed to zero phase and were displayed using SEG (Society for Exploration Geologists) reversed polarity, where an increase in acoustic impedance is represented by a positive (peak) reflection event. They have a dominant frequency of 30 Hz for the study interval of interest, yielding a vertical resolution of 18.75 m ($\lambda/4$) and a detection of 3 m ($\lambda/25$). No well data are available to authors, since most of them are still being kept confidential.

The present study is based on classical 2D seismic facies analysis (section-view-based interpretation, Vail et al. 1977) and 3D seismic geomorphology approach (plan-view-based interpretation, Posamentier and Kolla 2003), through which seismic stratigraphy and geomorphology of the interpreted net-depositional cyclic steps are quantitatively delineated in three dimensions. The root-mean-square (RMS) attribute calculates the square root of the sum of time-domain energy (square of the amplitude), affording high amplitudes the maximum opportunity to stand out from the background accumulation. RMS amplitude maps were extracted following the hanging horizon of T_{wave} (yellow line in Fig. 2b). They are employed to delineate the 3D architectures and plan-view distribution patterns of the Bengal net-depositional cyclic steps.

In addition, individual undulating bedforms documented in the present study contain three discrete, geometrically defined compartments, namely steep headcuts (lee sides) and flat or gently sloping stoss (upcurrent) sides, with a bed pool or depression in between (Fig. 3a; Cartigny et al. 2011; Covault et al. 2014). Bengal wave-like features, therefore, have been quantified, in terms of: (1) width and height (W and H, respectively) (Fig. 3b), (2) lengths of lee faces, stoss sides, and hydraulic jumps (L_{lee}, L_{stoss}, and L_{jump}, respectively) (Fig. 3b), (3) slopes of lee flanks and stoss sides (β and α, respectively) (Fig. 3b), (4) aspect ratio (W/H) (Fig. 3b), and (5) length of the crest line (P_l) (Fig. 2a). Please refer to Figs. 2a and 3b for a schematic illustration of how to measure these morphologic parameters. Our measurements of these parameters are not compacted; however, morphometrics determined by decompacted measurements are not large enough to warrant a different interpretation (Li and Gong 2018).

4 3D seismic stratigraphy and geomorphology of the Bengal undulating bedforms

Two fields of undulating bedforms were recognized in the study area in the Bay of Bengal (Figs. 2a, 4, 5, 6). Seismic stratigraphy, together with seismic geomorphology, has helped decipher and characterize them, in terms of

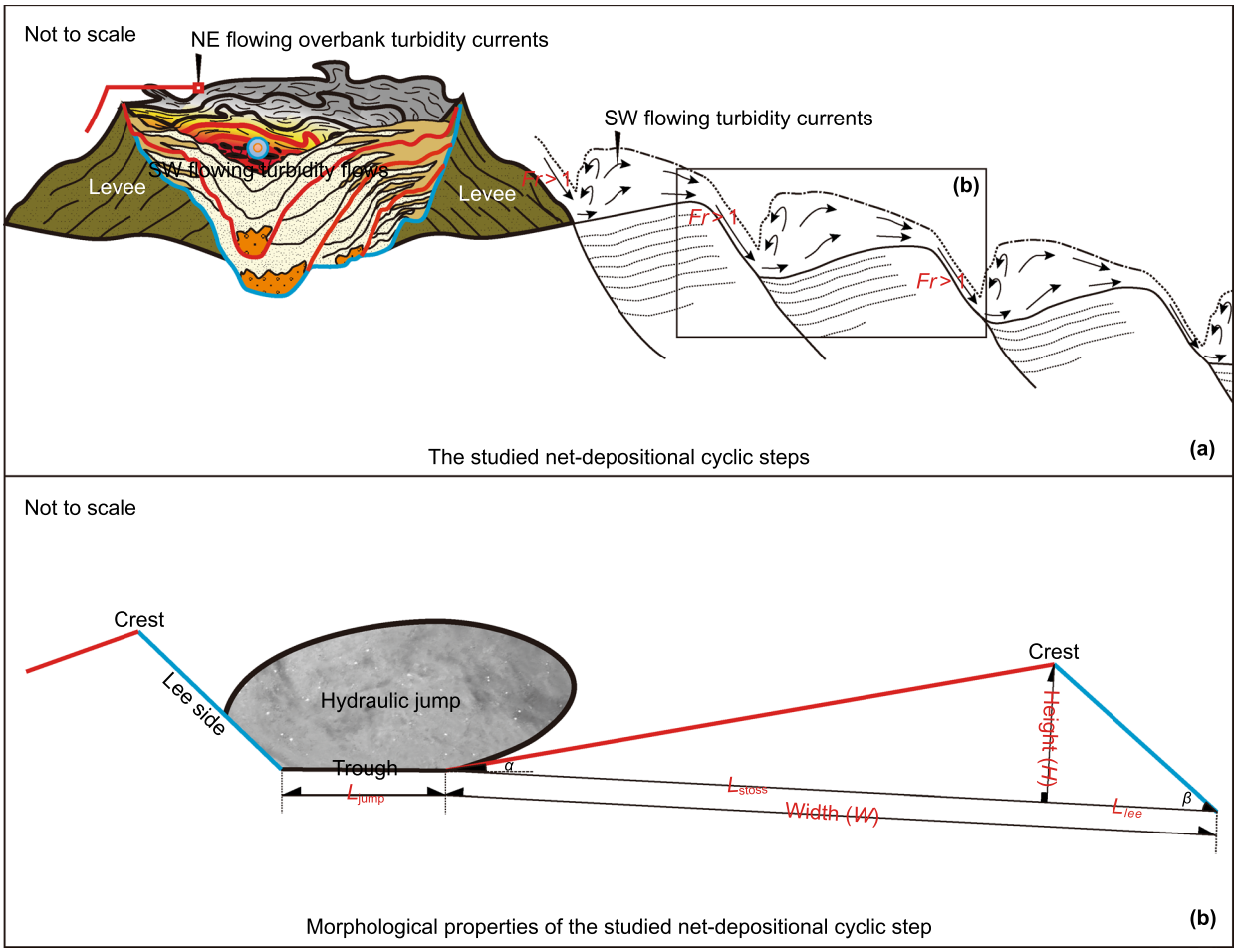

Fig. 3 **a** Schematic illustration of the relationship of directions of turbidity currents forming the Bengal undulating bedforms to submarine channel turbidity currents and their concomitant overbank turbidity flows. Note that overbank turbidity currents had flow directions perpendicular to the directions of the inferred turbidity currents involved in the construction of the Bengal undulating bedforms, suggesting that Bengal undulating bedforms could not be related to overbank turbidity currents. **b** Schematic illustration of morphologic parameters of individual cyclic steps (i.e., W = cyclic step width; H = cyclic step height; W/H = aspect ratio; L_{lee} = length of lee face; L_{stoss} = length of stoss face; L_{jump} = length of hydraulic jump; β = slope of lee flank; and α = slope of stoss side)

morphological properties, planform patterns, and architectural styles.

4.1 Morphometric properties of Bengal undulating bedforms

Undulating bedforms in field 1 cover an area of 150 km^2, while their counterparts in field 2 occupy an area of 110 km^2 (Figs. 2a, 5, 6; Tables 1, 2). Undulating bedforms in field 1 have W of 1241 to 2066 m (averaging 1626 m), H of 14 to 28 m (averaging 18 m), W/H of 58 to 138 (averaging 96), and P_l of 0.77 to 6.51 km (averaging 4.85 km) (Figs. 7a, 8a; Table 1), while their counterparts in field 2 are 587 to 1034 m (averaging 847 m) in W, 9 to 17 m (averaging 13 m) in H, 41 to 91 (averaging 68) in W/H, and 0.64 to 3.72 km (averaging 2.74 km) in P_l (Figs. 7a, 8a; Table 2). Individual undulating bedforms in both fields 1 and 2 contain three discrete, geometrically defined compartments, namely lee (downcurrent) flanks and stoss (upcurrent) flanks, with a bed pool (hydraulic jumps) in between (Fig. 3). Lee flanks of undulating bedforms in field 1 are 0.39° to 1.18° (averaging 0.69°) in slope gradients (β) and 183 to 419 m (averaging 318 m) in lengths (L_{lee}), while their stoss flanks are 0.12° to 0.27° (averaging 0.20°) in slope gradients (α) and 886 to 1399 m (averaging 1053 m) in lengths (L_{stoss}) (Figs. 7b, 8b; Table 1). Lee flanks of undulating bedforms in field 1 are, thus, 3 to 4 times steeper and 3 to 4 times shorter than their stoss sides. Troughs of undulating bedforms in field 1 have lengths (L_{jump}) of 52 to 484 m, with a mean value of L_{jump} = 256 m (Fig. 8a; Tables 1, 2). Moreover, lee sides of the Bengal undulating bedforms in field 2 have β of 0.28° to 1.19° (averaging 0.71°) and L_{lee} of 117 m to

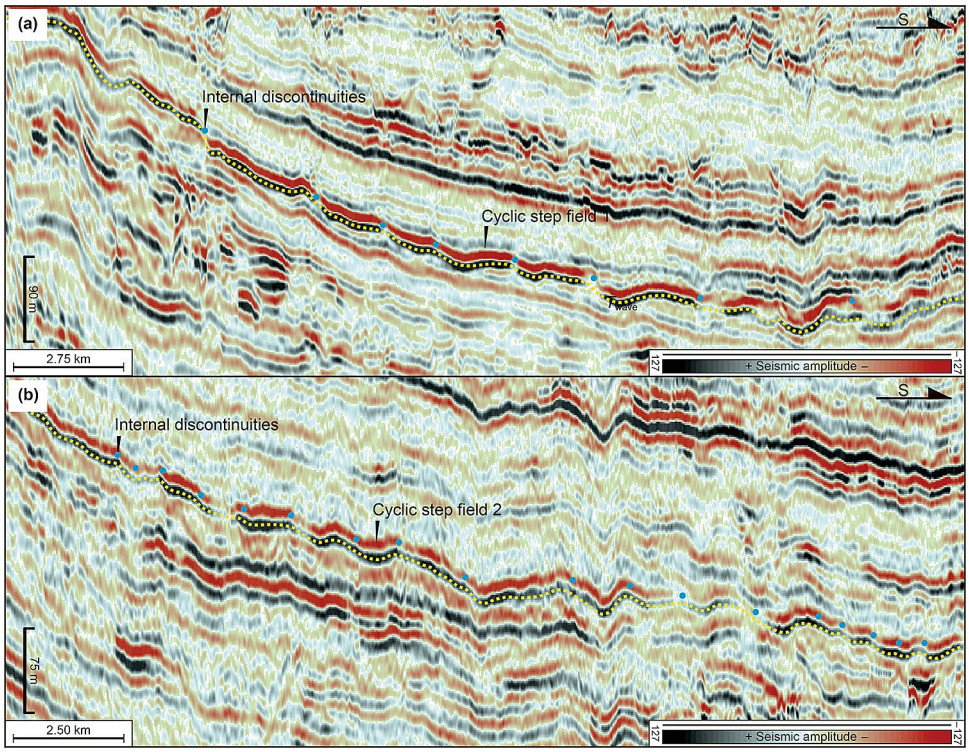

Fig. 4 Seismic sections (line locations shown in Fig. 2a) showing cross-sectional seismic expression of Pliocene undulating bedforms in fields 1 and 2 in Rakhine Basin (**a** and **b** panels, respectively). Note that the shown undulating bedforms are seismically imaged as rhythmically undulating, northward dipping, erosive, discontinuous reflections

232 m (averaging 171 m), while their stoss sides have α of 0.10° to 0.25° (averaging 0.20°) and L_{stoss} of 410 to 710 m (averaging 569 m) (Figs. 7b, 8b; Table 2). Stoss sides of undulating bedforms in field 2 are, thus, 3 to 4 times gentler and 3 to 4 times longer than their lee sides. Troughs of undulating bedforms in field 2 have L_{jump} of 30 to 188 m, with a mean value of $L_{jump} = 106$ m (Fig. 8a; Table 2). In addition, through the comparison of morphometric properties of two areas of Bengal undulating bedforms (i.e., the comparison between Tables 1 and 2), it could be found that undulating bedforms in field 1 have much larger scales than those in the field 2. Except the slopes of lee flanks and stoss sides (β and α, respectively) are comparable between these two fields, other morphometric properties of undulating bedforms all have larger values in filed 1 compared with those in field 2.

4.2 Architectural styles of Bengal wave-like features

In section view, lee flanks of the interpreted undulating bedforms in fields 1 and 2 are, overall, thinner (i.e., 10 to 15 m) than their stoss sides, and are seismically imaged as rhythmically undulating, northward dipping, erosive, discontinuous reflections (dots in Fig. 4). Stoss flanks of the studied undulating bedforms in fields 1 and 2, in contrast, are thicker (i.e., 15 to 20 m) than their lee sides, and are seismically expressed themselves as rhythmically undulating, southward dipping, tabular, continuous reflectors (Fig. 4). Sediment deposition, therefore, occurs preferentially on the downstream (stoss sides, southward) flanks, whereas low deposition, bypassing, and even erosion predominate on the upstream (lee sides, northward) flanks, giving rise to clear upstream-migrating growth patterns (Figs. 3, 4). In the depositional strike view, Bengal wave-like bedforms as documented in this study are seismically manifested as parallel, high-amplitude, continuous reflections (Fig. 9a, b).

4.3 Planform patterns of Bengal undulating bedforms

In plan view, Bengal wave-like features in fields 1 and 2 collectively appear in RMS attribute-extraction maps as strike-elongated, crescentic features (Figs. 5, 6, 10). They eventually disappear on time slices taken 90 ms above and below T_{wave} (Fig. 11a, b, respectively), on which channel-levee systems and mass-transport complexes are seen. Undulating bedforms in field 1 are separated from their counterparts in field 2 by sinuous deep-water channels imaged as single, narrow, north–south trending, dark-colored bands on RMS attribute-extraction maps (Figs. 5, 6), and are imaged

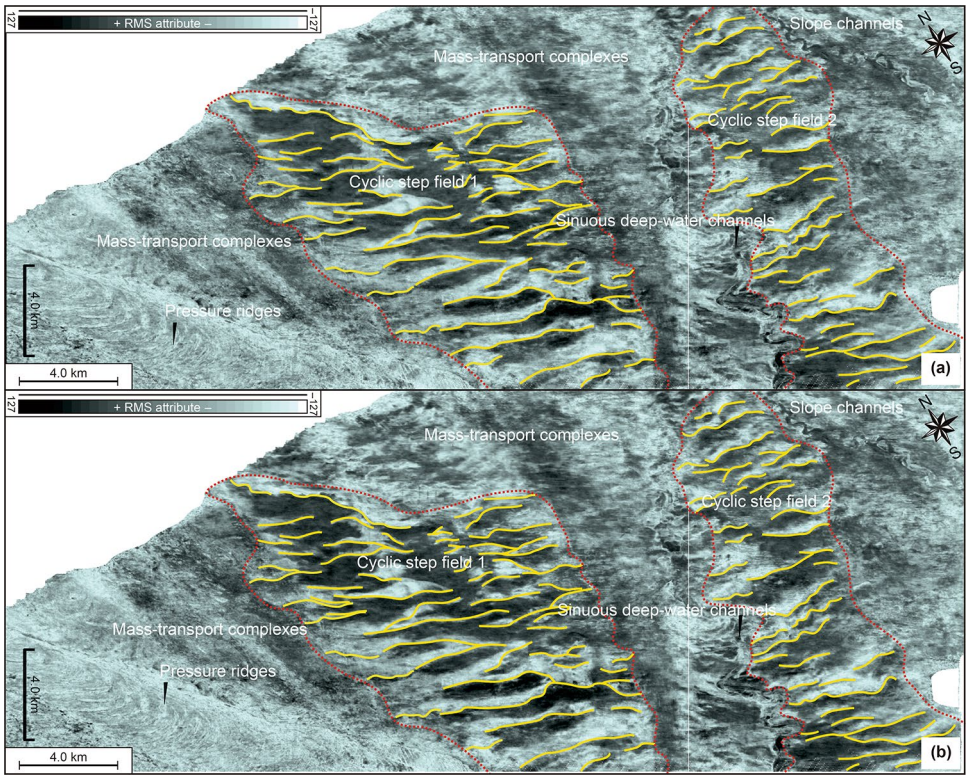

Fig. 5 RMS-extraction maps taken 2 ms above and below the hanging horizon of T_{wave} (**a** and **b** panels, respectively) (see the stratigraphic position of T_{wave} in Figs. 2b and 4) illustrating plan-view geomorphological expression of Pliocene undulating bedforms in fields 1 and 2 in Rakhine Basin (upper and lower panels, respectively). Note that the shown undulating bedforms are imaged as strike-elongated, crescentic bedforms with straight to moderately sinuous crest lines

as U-shaped scours filled by high-amplitude discontinuous reflections on strike-oriented seismic sections (Fig. 9a, b).

Crest lines of Bengal undulating bedforms in field 1 are continuous along the depositional strike for approximately 0.8 to 6.5 km (averaging 4.8 km), while crest lines of Bengal undulating bedforms in field 2 are approximately 0.6 to 3.7 km (averaging 2.7 km) in plan-view length (Figs. 5, 6, 10; Tables 1, 2). Crest lines of the documented undulating bedforms in fields 1 and 2 are either linear or moderately sinuous and show regular bifurcation (undulating lines in Figs. 5, 6, 10). They are collectively oriented parallel or subparallel to the depositional strike of the regional slope, but are roughly orthogonal to the orientation of contemporaneous sinuous deep-water channels (Figs. 5, 6, 10).

5 Formational mechanisms of the Bengal undulating bedforms

At least, four main mechanisms have been proposed to explain the formation and origin of giant, rhythmically undulating sedimentary features (e.g., Migeon et al. 2000; Masson et al. 2002; Normark et al. 2002; Wynn and Stow 2002; Fildani et al. 2006; Paull et al. 2010; Symons et al. 2016). They are used to examine the geneses of the aforementioned undulating bedforms recognized in the Bay of Bengal.

5.1 Can Bengal wave-like bedforms be related to internal tides or waves?

Previous studies have suggested that the integrated effects of internal tides and/or waves are able to produce some crescent-shaped bedforms (e.g., Smith et al. 2007; Xu et al. 2008; Paull et al. 2010). For example, Smith et al. (2007), Xu et al. (2008), and Paull et al. (2010) have ascribed the crescent-shaped bedforms in the Monterey Canyon, offshore California to internal tides and/or waves. The documented undulating bedforms in the Rakhine Basin also have crescent-shaped crests that are continuous along the depositional strike for 0.6 to 6.5 km, with an average length of approximately 3.8 km (Figs. 5, 6, 10; Tables 1, 2). However, if the Bengal crescent-shaped bedforms were formed by internal waves and/or tides, they would commonly migrate in a downstream direction and should display downstream-dipping internal structures with thick depositional upstream sides, as typified by those observed in Monterey Canyon

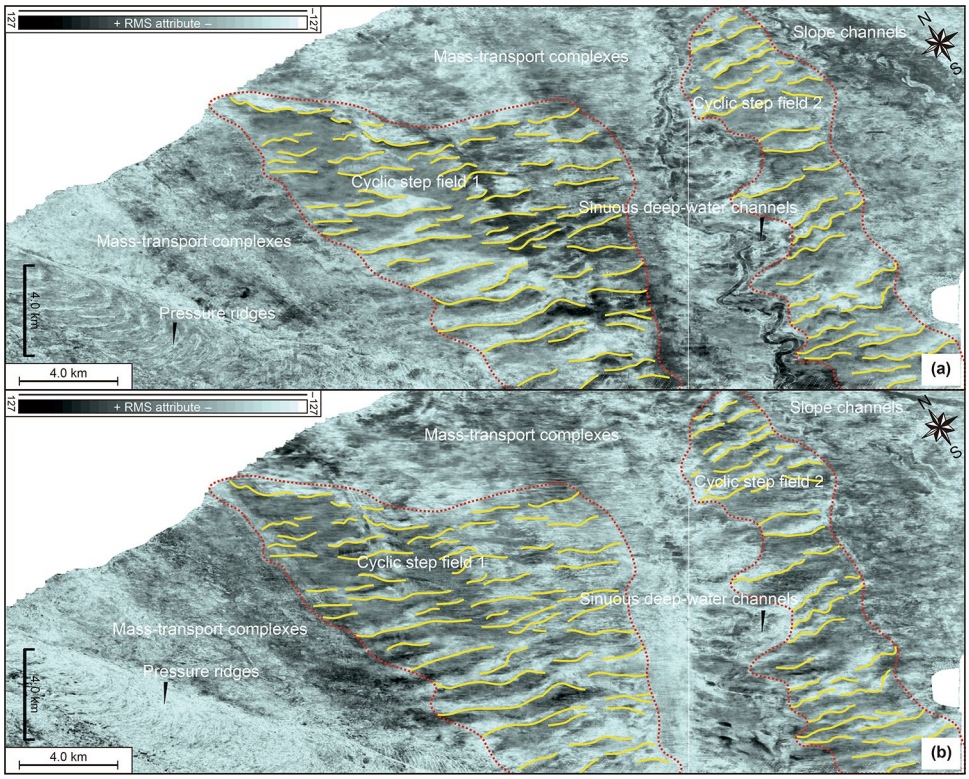

Fig. 6 RMS-extraction maps taken 20 ms above and below the hanging horizon of T_{wave} (**a** and **b**, respectively) (see the stratigraphic position of T_{wave} in Figs. 2b and 4) illustrating plan-view geomorphological manifestations of undulating bedforms in fields 1 and 2

Table 1 Morphometric properties of the studied net-depositional undulating bedforms in field 1

Query	W	H	L_{lee}	L_{stoss}	L_{jump}	W/H	β	α	P_l	Area
Minimum	1241 m	14 m	183 m	886 m	52 m	58	0.39°	0.12°	0.77 km	150 km^2
Maximum	2066 m	28 m	419 m	1399 m	484 m	139	1.18°	0.27°	6.51 km	
Mean	1626 m	18 m	318 m	1053 m	256 m	96	0.69°	0.20°	4.85 km	
Standard deviation	±241	±4	±64	±132	±16	±20	±0.19	±0.05	N/A	

W = wave width, H = wave height, L_{lee} = length of lee side, L_{stoss} = length of stoss side, L_{jump} = length of hydraulic jump, W/H = aspect ratio, β = slope gradient of lee side, α = slope gradient of stoss side, and P_l = plan-view length. Please refer to Figs. 2a and 3b for a schematic illustration of how to measure these morphologic parameters

Table 2 Morphometric properties of the documented undulating bedforms in field 2

Query	W	H	L_{lee}	L_{stoss}	L_{jump}	W/H	β	α	P_l	Area
Minimum	587 m	9 m	117 m	410 m	30 m	42	0.28°	0.10°	0.64 km	110 km^2
Maximum	1034 m	17 m	232 m	710 m	188 m	91	1.19°	0.25°	3.72 km	
Mean	847 m	13 m	171 m	569 m	106 m	68	0.71°	0.20°	2.74 km	
Standard deviation	±241	±2	±39	±132	±42	±15	±0.26	±0.06	N/A	

W = wave width, H = wave height, L_{lee} = length of lee side, L_{stoss} = length of stoss side, L_{jump} = length of hydraulic jump, W/H = aspect ratio, β = slope gradient of lee side, α = slope gradient of stoss side, and P_l = plan-view length. Please refer to Fig. 3b for a schematic illustration of how to measure these morphologic parameters

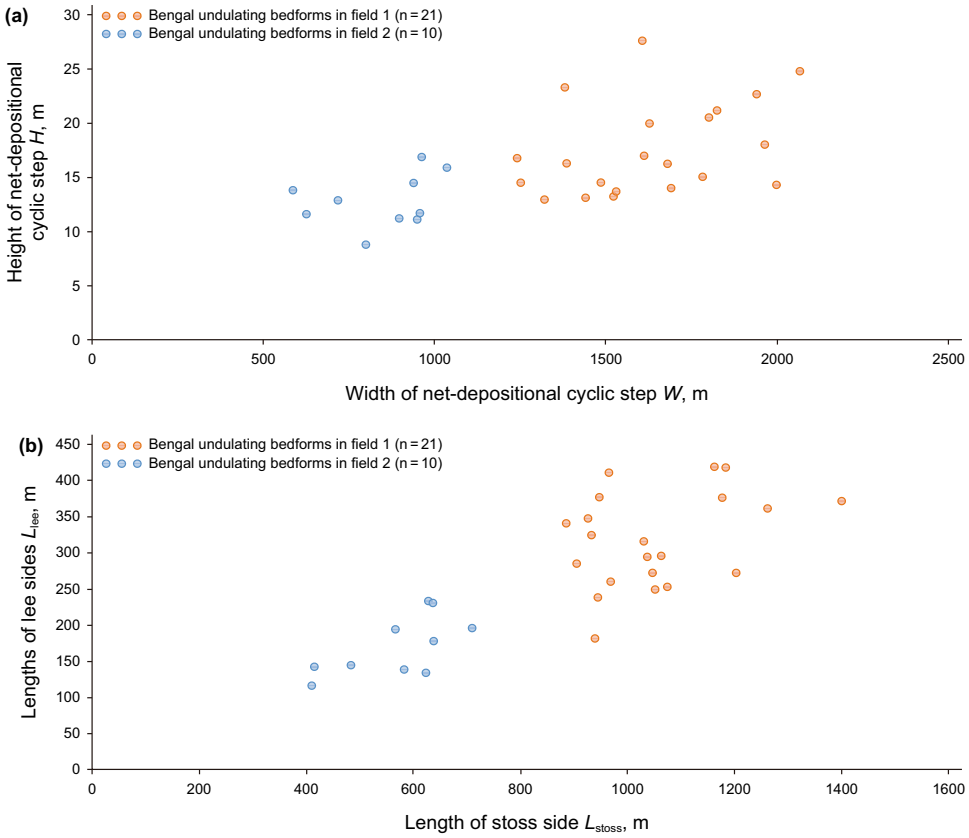

Fig. 7 Scatterplots of W against H and L_{stoss} against L_{lee} for Pliocene Bengal undulating bedforms (**a** and **b** panels, respectively)

(Smith et al. 2007; Xu et al. 2008; Paull et al. 2010). However, the possibility of internal tides and waves as a formational mechanism for the Bengal crescentic to undulatory bedforms is here not favored by: (i) upstream-dipping internal structures with thick depositional stoss sides and (ii) upstream migration, as suggested by the erosionally truncated upstream sides (Fig. 4). Moreover, internal waves or tides occur most frequently on continental shelves and adjacent areas (e.g., Pomar et al. 2012). However, the Bengal crescentic to undulatory bedforms documented herein were contemporaneous with sinuous deep-water channels (Figs. 5, 6, 10), which, in turn, suggests a deep-water origin, further suggesting that Bengal undulating bedforms cannot be related to internal waves or tides occurring most frequently on shallow-water shelves and adjacent areas.

5.2 Can Bengal undulating bedforms be ascribed to bottom (contour) currents?

Large-scale bottom-current sediment waves are one of the most distinct and widespread phenomena in deep-water settings, and commonly occupy huge areas of sea floor (e.g., > 1000 km^2) (e.g., Wynn and Stow 2002; Symons et al. 2016). Such rhythmically undulating bedforms typically occur in areas swept by bottom (contour) currents, especially where there is a change in slope gradients (e.g., the base of continental rise) (e.g., Masson et al. 2002; MacLachlan et al. 2008). The possibility of bottom (contour) currents as a formational mechanism of Pliocene Bengal wave-like features is, however, ruled out by: (i) asymmetrical cross-sections with internal discontinuities (blue dots in Fig. 4) and (ii) moderately sinuous wave crests with regular bifurcation (wavy lines in Figs. 5, 6, 10). In marked contrast to the Bengal undulating bedforms, well-documented bottom-current sediment waves are commonly more symmetrical with continuous, parallel to subparallel internal seismic-reflection configurations, and have wave crests that are parallel or subparallel to bathymetric contours and rarely bifurcate (e.g., Masson et al. 2002; Hohbein and Cartwright 2006; MacLachlan et al. 2008).

5.3 Can Bengal undulating bedforms be ascribed to overbank turbidity currents?

Asymmetric, upstream-migrating sediment waves are also found to occur on submarine channel levees, giving rise to overbank turbidity current sediment waves (Normark et al. 2002; Wynn and Stow 2002). Driven by Coriolis forces, they

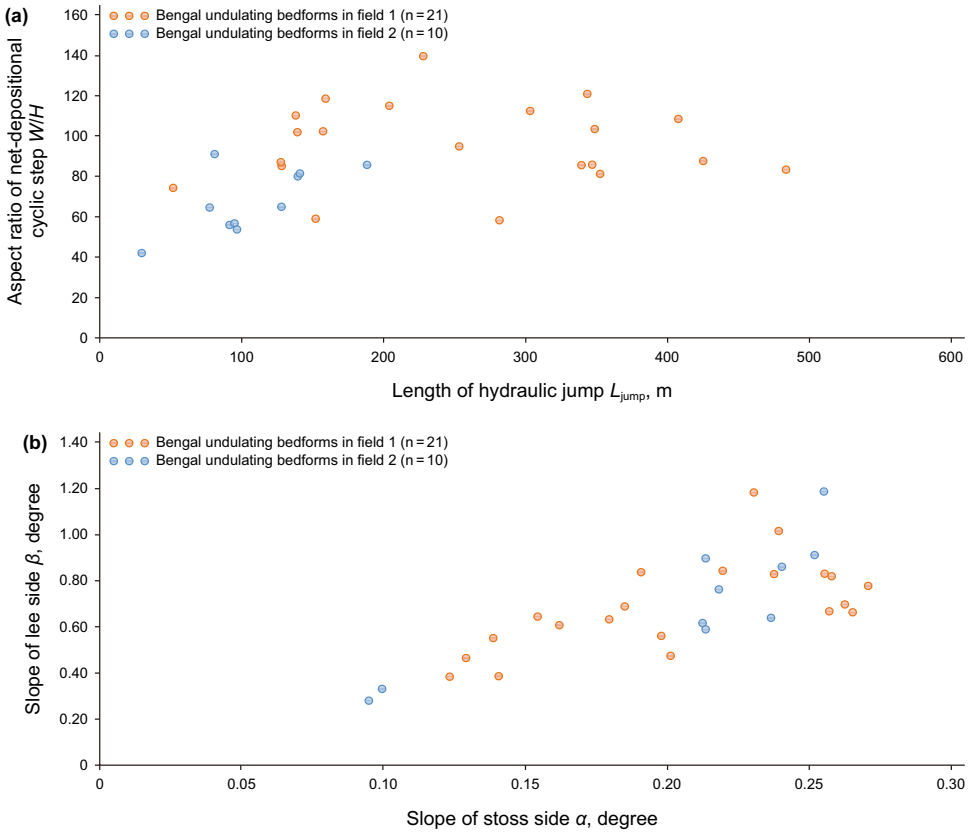

Fig. 8 Cross-plots of L_{jump} versus *W/H* and α versus *B* for Pliocene Bengal undulating bedforms (**a** and **b** panels, respectively)

were typically developed on the right-hand levees of deep-water channel systems in the northern hemisphere (left-hand levees in the southern hemisphere) (Normark et al. 2002). Overbank turbidity currents have been proposed to explain the origin of sediment waves in overbank regions of Var canyon in the Ligurian Basin, northwestern Mediterranean (Migeon et al. 2000), Monterey and Ascension canyons (Normark et al. 2002), the Shepard Bend of the Monterey Canyon (Fildani et al. 2006), the Eel Canyon (Lamb et al. 2008) and the San Mateo channel (Covault et al. 2014) offshore California, USA, and West Penghu submarine canyons off southwestern Taiwan (Zhong et al. 2015). The documented Bengal undulatory bedforms were dissected by sinuous deep-water channels, occur on overbank regions of the seismically well-imaged channels (Figs. 5, 6, 10), and are upstream migrating (Fig. 4). One, thereby, may wonder whether can Bengal undulating bedforms be ascribed to overbank turbidity currents. As shown in Figs. 5 and 6, sinuous deep-water channels seen as narrow, tortuous, trending southwestward trending high RMS-attribute ribbons are oriented perpendicular to the crest lines of Bengal undulating bedforms. The channel-axis perpendicular orientation of crest lines of the Bengal undulating bedforms, in turn, suggests that Bengal undulating bedforms were not constructed by northeastern or northwestern flowing overbank turbidity currents (Figs. 3a, 5, 6). In marked contrast to such planform patterns, crest lines of well-documented overbank turbidity current sediment waves typically align parallel or subparallel to the channel axis, making them oriented roughly perpendicular to the direction of overbank turbidity currents (e.g., Migeon et al. 2000; Normark et al. 2002).

5.4 Can Bengal undulating bedforms be related to unconfined turbidity currents?

Similar to bottom-current sediment waves, turbidity current sediment waves are also one of the most frequently described undulatory bedforms in deep-water settings, and are also widespread on sea floor (e.g., Wynn and Stow 2002; Symons et al. 2016). In plan view, wave crests of the Bengal undulating bedforms regularly bifurcate and are roughly perpendicular to directions of southwestward-flowing turbidity currents (Figs. 5, 6). The same planform patterns have also been observed in turbidity current sediment waves on the continental slope and rise of the northern Canary Island margin (Wynn et al. 2000a), the slope of the western Canary Islands (Wynn et al. 2000b), the southern margin of the Orinoco Valley (Ercilla et al. 2002),

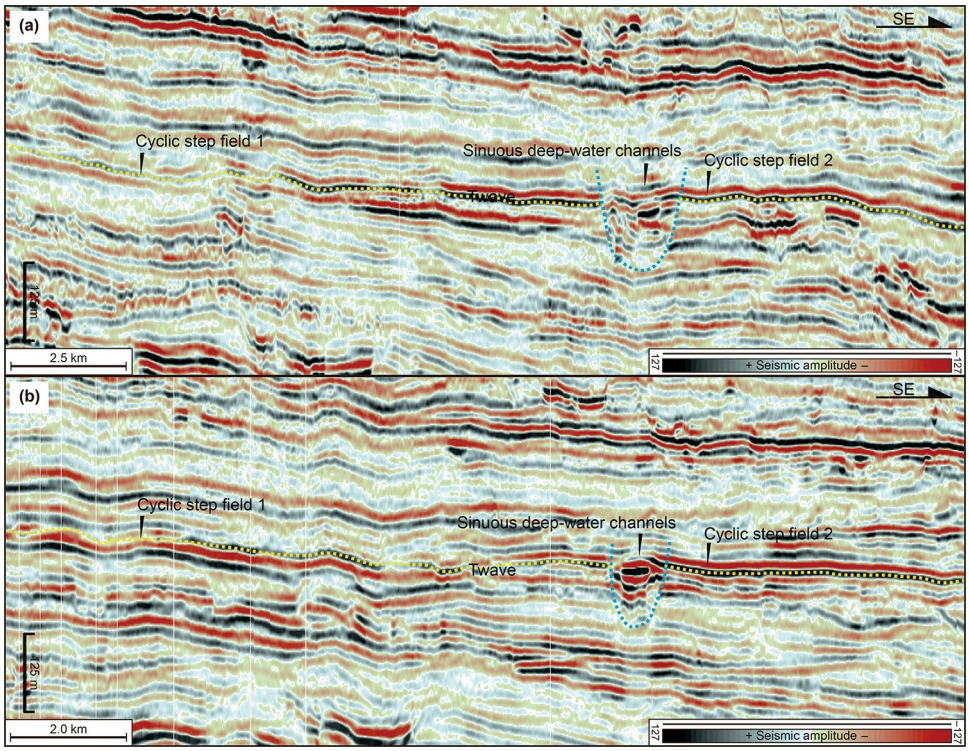

Fig. 9 Seismic transects (see line locations in Fig. 2a) showing depositional strike-view seismic appearance of wave-like features fields 1 and 2 (**a** and **b** panels, respectively). Note that Pliocene Bengal undulating bedforms were dissected by sinuous deep-water channels

the Shepard Meander of the Monterey Fan (Fildani et al. 2006), and the northeastern South China Sea slope (Gong et al. 2012). In cross-sectional view, the Bengal undulating bedforms as studied in this work exhibit strongly asymmetric cross-sections with internal discontinuities and upstream-migrating growth patterns, in which their upstream flanks are steeper and shorter than their downstream flanks (Fig. 4). Undulating asymmetric cross-sections with internal discontinuities and upstream-migrating growth patterns are two characteristics of turbidity current sediment waves (Wynn and Stow 2002; Ercilla et al. 2002; Gong et al. 2012) and are also consistent with morphological properties of cyclic steps observed from seismic and bathymetric datasets (e.g., Fildani et al. 2006; Lamb et al. 2008; Heiniö and Davies 2009; Zhong et al. 2015; Fricke et al. 2015; Normandeau et al. 2016), outcrop datasets (e.g., Ponce and Carmona 2011), and from numerical (Kostic and Parker 2006; Cartigny et al. 2011; Kostic 2014; Covault et al. 2014, 2017; Vellinga et al. 2018), and physical experiments (Cartigny et al. 2014; Kostic 2014). Similar to fine-grained sediment waves crested by unconfined turbidity currents (e.g., Migeon et al. 2000; Ercilla et al. 2002; Normark et al. 2002; Fildani et al. 2006), the Bengal turbidity current sediment waves occur in unconfined settings (Figs. 5, 6, 10), suggesting that we can further relate them to unconfined turbidity currents.

6 Numerical computations of parameters of unconfined turbidity currents forming Bengal undulating bedforms

As discussed above, the genesis of the documented Bengal undulating bedforms is ascribed to unconfined turbidity currents, which have been parameterized in this section, in terms of internal Froude numbers, flow thickness, and flow velocities.

6.1 Froude numbers of Bengal undulating bedform-forming turbidity currents

Bowen et al. (1984) have suggested that internal Froude numbers (Fr) are related to the slope gradient (β), the drag coefficient at the bed (Cf), and the entrainment coefficient at the upper interface (E), such that:

$$\mathrm{Fr} = \sqrt{\sin\beta/(Cf + E)} \tag{1}$$

Previous studies have shown that the drag coefficient in unconfined turbidity currents (Cf) varies from 0.0035 to 0.004, and that entrainment coefficient (E) for most turbidity currents ranges from 0.0005 to 0.006 (e.g., Bowen et al. 1984; Ercilla et al. 2002). Ercilla et al. (2002) have

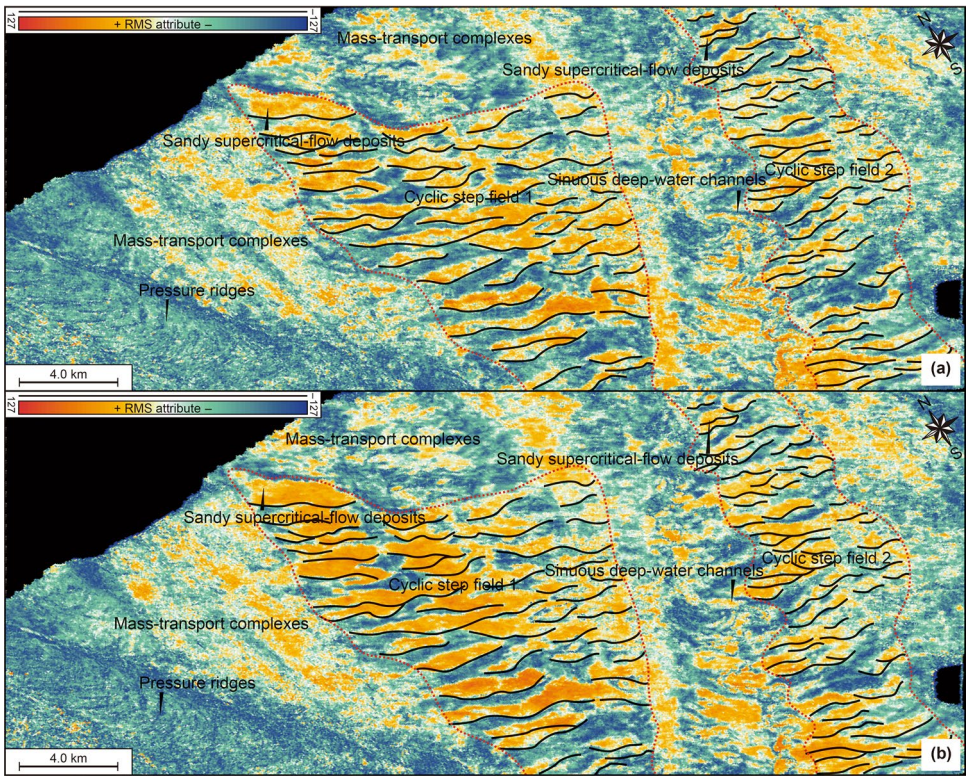

Fig. 10 RMS attribute-extraction maps showing the distribution of higher (sandier, yellow and orange) versus lower (muddier, green and blue) RMS attributes of the studied wave-like bedforms in fields 1 and 2. Note that higher RMS attributes display closely spaced, long and linear, isolated, strike-elongated distribution patterns. Time windows for RMS attribute-extraction maps shown in this figure are 15 ms above and below the hanging horizon of T_{wave} (**a** and **b** panels, respectively)

suggested that turbidity currents forming turbidity current sediment waves on the southern Orinoco margin had $Cf + E = 0.005$. These values were then plugged into Eq. 1, resulting in Fr of turbidity currents forming the Bengal undulating features (Fig. 12a, b; Table 3). More specifically, Fr of turbidity currents on lee sides of wave-like features were estimated to range from 1.53 to 2.27 (averaging 1.84) and 1.65 to 2.16 (averaging 1.84), respectively (Fig. 12a; Table 3). Fr of turbidity flows on stoss sides of wave-like bedforms in fields 1 and 2 were computed to vary from 0.66 to 0.97 (averaging 0.84) and 0.58 to 0.94 (averaging 0.83), respectively (Fig. 12b; Table 3). In all of these cases, Fr of turbidity flows on lee sides are higher than 1 (i.e., supercritical-flow conditions), whereas Fr of turbidity currents across stoss flanks are lower than 1 (subcritical flow conditions) (Fig. 12; Table 3). Our results are in agreement with previous research on unconfined turbidity currents involved in the construction of sediment waves on the Monterey fan levees (Normark et al. 1980), the continental slope and rise of the northern Canary Island margin (Wynn et al. 2000a), the slope of the western Canary Islands (Wynn et al. 2000b), and the southern margin of the Orinoco Valley (Ercilla et al. 2002).

6.2 Thicknesses of turbidity currents forming Bengal undulating bedforms (*h*)

Normark et al. (1980) have suggested that flow thicknesses (h) are related to wavelength (L) and internal Froude number (Fr) through Eq. 2:

$$h = \frac{L}{2\pi \mathrm{Fr}^2} \tag{2}$$

Normark's model (i.e., Eq. 2) has been validated by Kubo and Nakajima (2002), Lee et al. (2002), and Kostic (2014). Wave-like features in both fields 1 and 2 have wavelengths ranging from 1241 to 2066 m (averaging 1626 m) and 587 to 1034 m (averaging 847 m), respectively. Using Eq. 2 and the computed results of Fr as computed by Eq. 1, turbidity currents forming undulatory bedforms in both fields 1 and 2 had h ranging from 39 to 122 m (averaging 79 m) and 2.28 to 55 m (averaging 41 m), respectively (Fig. 12). These values are comparable with those estimated in the previous research on paleoflow parameters of turbidity currents forming large-scale sediment waves in unconfined settings (e.g., Normark et al. 1980; Wynn et al. 2000a, b; Ercilla et al. 2002).

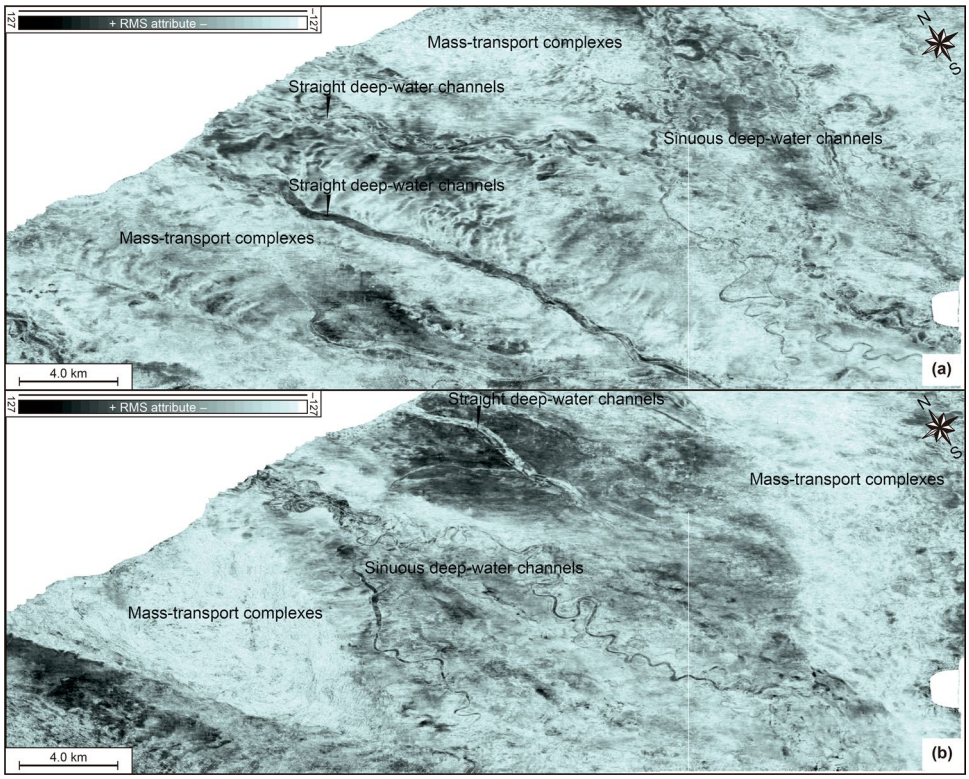

Fig. 11 RMS attribute-extraction maps taken 90 ms above and below the hanging horizon of T_{wave} (**a** and **b** panels, respectively) (see the stratigraphic position of T_{wave} in Figs. 2b and 4) illustrating plan-view geomorphological appearance of channel-levee systems and mass-transport complexes. Note that wave-like bedforms related to supercritical-to-subcritical flow transformations through internal hydraulic jumps expressed on time slices of Figs. 5 and 6 are here absent

6.3 Velocities of turbidity currents forming Bengal undulating bedforms (*u*)

Piper and Savoye (1993) and Ercilla et al. (2002) have suggested that flow velocities of turbidity currents (u) are related to Fr through Eq. 3:

$$u = \sqrt{\left[\left(\rho_t - \rho_w\right)/\rho_w\right] Cgh}\mathrm{Fr} \tag{3}$$

where ρ_t is the density of the turbidity currents, ρ_w is the density of the ambient seawater (1027 kg/m^3), C is the volume concentration, and g is the acceleration of gravity (9.8 m/s^2). C is highly variable and is one of the most poorly constrained variables in turbidity current modeling (Ercilla et al. 2002). Existing database and previous studies suggest that C of fine-grained, unconfined turbidity currents commonly range from 0.00005 to 0.50 (Bowen et al. 1984; Piper and Savoye 1993; Ercilla et al. 2002; Sequeiros 2012). Sequeiros (2012) has suggested that typical values for turbidity flows at field scale are $C < 0.45$ for siliciclastic material with a grain density of 2650 kg/m^3. When these input parameters were entered into Eq. 3, it can be shown that: (i) u of flows on lee sides of Bengal wave-like features in both fields 1 and 2 ranges from 2.70 to 3.98 m/s (averaging 3.24 m/s) and 2.90 to 3.80 m/s (averaging 3.24 m/s), respectively and (ii) that u of flows over stoss sides of Bengal undulatory bedforms in both fields 1 and 2 varies from 2.50 to 3.05 m/s (averaging 2.82 m/s) and 2.35 to 3.00 m/s (averaging 2.81 m/s), respectively (Fig. 13; Table 3). In all of these cases, flows on lee faces tend to be faster (reported as u of 2.70 to 3.98 m/s, with a mean value of $u = 3.24$ m/s), whereas those on stoss sides appear to be slower (reported as u of 2.35 to 3.05 m/s, with a mean value of $u = 2.82$ m/s) (Fig. 13; Table 3). Turbidity currents on lee flanks of Bengal wave-like features, therefore, had velocities and Froude numbers that are, respectively, 1 to 2 and 2 to 3 times higher than those on stoss sides. These values of u are in agreement with the paleoflow reconstruction of unconfined turbidity currents forming large-scale turbidity sediment waves (e.g., Normark et al. 1980; Wynn et al. 2000a, b; Ercilla et al. 2002).

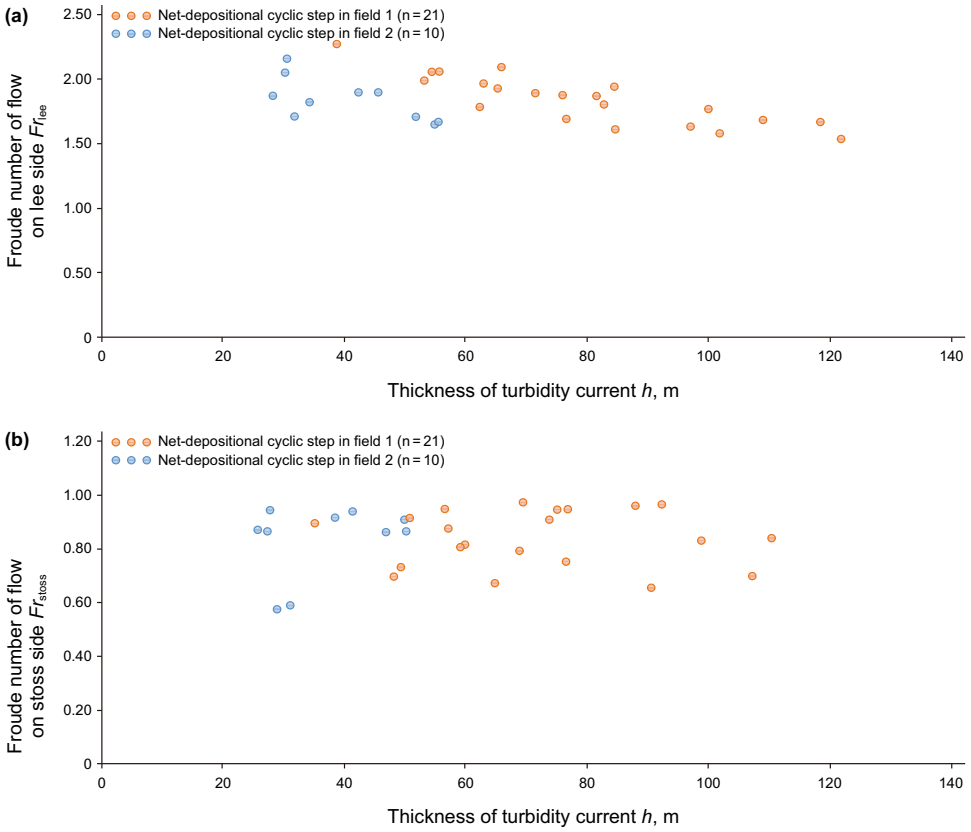

Fig. 12 Scatterplots of h against Fr_{lee} and h against Fr_{stoss} for Bengal undulatory bedforms related to supercritical-to-subcritical flow transformations through internal hydraulic jumps (**a** and **b** panels, respectively)

Table 3 Estimated parameters of unconfined turbidity currents on lee and stoss sides of the documented net-depositional cyclic steps in the Bay of Bengal

Query	Flows on lee sides				Flows on stoss sides			
	Minimum	Maximum	Mean	Deviation	Minimum	Maximum	Mean	Deviation
Fr of flows in field 1	1.53	2.27	1.84	±0.19	0.66	0.97	0.84	±0.10
Fr of flows in field 2	1.65	2.16	1.84	±0.16	0.58	0.94	0.83	±0.13
u of flows in field 1 (m/s)	2.70	3.98	3.24	±0.33	2.50	3.05	2.82	±0.18
u of flows in field 2 (m/s)	2.90	3.80	3.24	±0.28	2.35	3.00	2.81	±0.23

Fr = internal Froude number and u = flow velocity

7 The classification of Bengal undulating bedforms

7.1 Flow dynamics of Bengal wave-like bedforms

The above computation of parameters of turbidity currents forming Bengal undulating features in both fields 1 and 2 suggests that turbidity flows on lee sides were faster (reported as u of 2.70 to 3.98 m/s, with a mean value of $u = 3.24$ m/s) and supercritical (represented by Fr of 1.53 to 2.27, with a mean value of Fr = 1.84), but that those across stoss flanks were slower (reported as u of 2.35 to 3.05 m/s, with a mean value of $u = 2.82$ m/s) and subcritical (represented by Fr of 0.58 to 0.97, with a mean value of Fr = 0.84) (Figs. 12, 13; Table 3). Lens-shaped trough of individual Bengal turbidite sediment waves, in contrast, marks a hydraulic jump from supercritical-to-subcritical turbidity currents (Fig. 3). Bengal undulating bedforms in both fields 1 and 2 were, thus, related to supercritical-to-subcritical flow transformations through internal hydraulic jumps, suggesting that they can be best interpreted to be

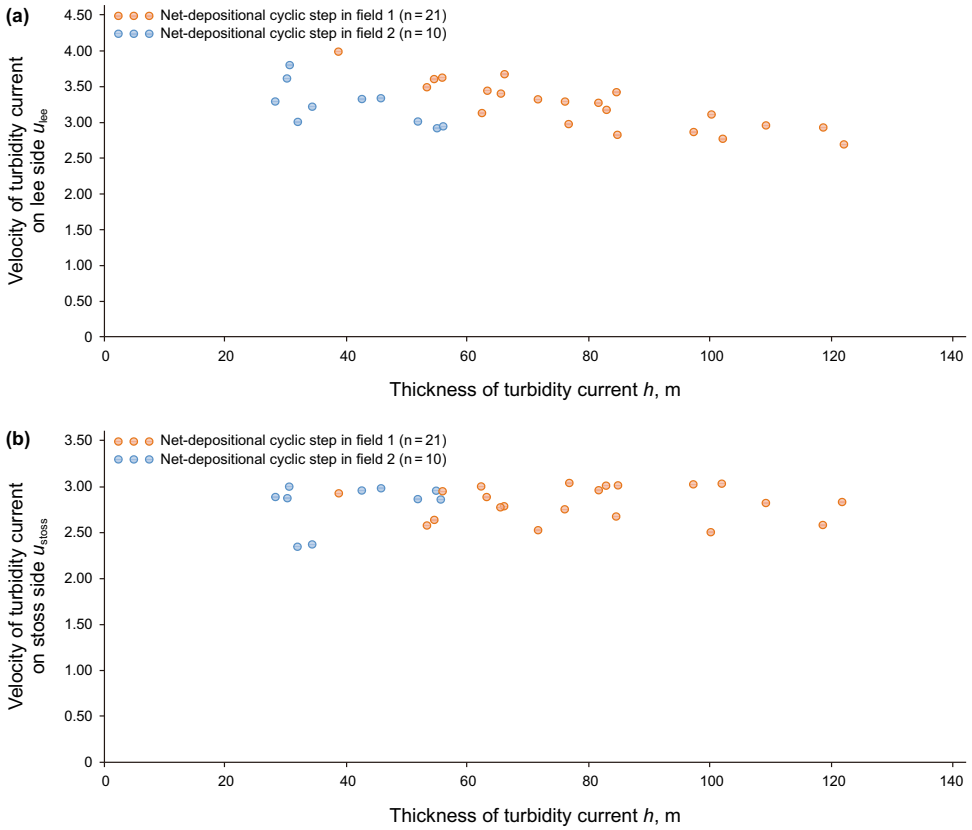

Fig. 13 Cross-plots of h versus u_{lee} and h versus u_{stoss} for Bengal undulatory bedforms related to supercritical-to-subcritical flow transformations through internal hydraulic jumps (**a** and **b** panels, respectively)

cyclic steps (e.g., Cartigny et al. 2011, 2014; Covault et al. 2017). Taki and Parker (2005), Fildani et al. (2006), Cartigny et al. (2011), Zhong et al. (2015), and Symons et al. (2016) have collectively suggested that turbidity currents may have passed from supercritical-to-subcritical flows on their passage across trains of long-wave, upstream-migrating bedforms that are common in regions of continent margins with high gradients and slope break. Cyclic steps, therefore, represent an alternative to the existing interpretations on the origin of wave-like features such as sediment waves (Fildani et al. 2006; Cartigny et al. 2011; Symons et al. 2016; Covault et al. 2017). Based on the direct monitoring of channelized turbidity currents known to be supercritical, Hughes Clarke (2016) has shown the first field-scale flow observations in support of a cyclic step origin of crescent-shaped, upstream-migrating bedforms. Similar to cyclic steps in less confined settings such as levee-overbank environments or channel-lobe transition zone (e.g., Wynn and Stow 2002; Cartigny et al. 2011; Kostic 2011; Symons et al. 2016; Covault et al. 2017), Bengal cyclic steps are also seen to occur on unconfined submarine environments of the continental slope in the Bay of Bengal (Figs. 1, 5, 6, 10, 11).

In addition, two formational mechanisms have been proposed to explain the origins of wave-like features such as sediment waves, including dunes and antidunes (e.g., Wynn and Stow 2002; Xu et al. 2008; Cartigny et al. 2011; Kostic 2011; Symons et al. 2016). Wave-like bedforms with downstream asymmetry and downslope migration have been interpreted as dunes created by subcritical flows (e.g., Xu et al. 2008), while those with upstream asymmetry and upstream migration were considered as antidunes formed by supercritical-to-subcritical flow transformations through internal hydraulic jumps (Normark et al. 2002). Bengal wave-like features also exhibit upstream asymmetrical geometries and upstream-migrating growth patterns as evidenced by the widespread occurrence of internal discontinuities on their downstream flanks (blue dots in Fig. 4a, b). The domination of erosion at lee sides of Bengal wave-like features (i.e., upstream asymmetrical geometries) strongly suggests that they are cyclic steps or antidunes.

7.2 The classification of Pliocene Bengal cyclic steps

Cyclic steps can be further divided into net-depositional and net-erosional categories, depending on whether the

dominant processes across the bedforms are erosional or depositional (e.g., Fildani et al. 2006; Kostic 2011; Zhong et al. 2015; Covault et al. 2014, 2017; Li and Gong 2018). Bengal cyclic steps in both fields 1 and 2 collectively have crests that are positive relative to the surrounding region of the seafloor (Figs. 2a, 5, 6), suggesting the predominant deposition of draping sediments (Symons et al. 2016). Such predominant deposition of draping sediments, in turn, suggests that turbidity currents forming Bengal sediment waves were, thus, dominated by deposition, indicating that Bengal cyclic steps in both fields 1 and 2 can be further classified as the net-depositional category. This hypothesis is also supported by conclusions reached by Kostic and Parker (2006), Fildani et al. (2006), Kostic (2011), Covault et al. (2017) and Symons et al. (2016), all of which collectively suggest that in many cases net-depositional cyclic steps take the form of upstream-migrating sediment waves. Fildani et al. (2006) applied the numerical model of Kostic and Parker (2006) to demonstrate that sediment waves on the outer levee of the Shepard Meander on the Monterey Fan to be the net-depositional cyclic steps. Daily bathymetric surveys of Squamish prodelta witnessed frequent (daily) upstream migration of crescentic sediment waves that were related to asymmetric net-depositional cyclic steps (Hughes Clarke et al. 2014; Hughes Clarke 2016).

8 Conceptual implications

The present work provides a novel context for sedimentologic interpretation, numerical models, and physical experiments of cyclic steps and related bedforms, and yields the following two main contributions.

Recent numerical and physical experiments have significantly increased and improved our understanding of supercritical-flow regimes, and have demonstrated that supercritical-flow phenomena are fairly common on our planet (e.g., Sun and Parker 2005; Fildani et al. 2006; Kostic et al. 2010; Cartigny et al. 2011, 2014; Kostic 2014). Net-depositional cyclic steps are widespread in turbidite systems and were particularly well developed on overbank depositional environments (Symons et al. 2016). However, there is still a shortage of 3D anatomy of them, especially where their 3D seismic stratigraphy and geomorphology can be examined (e.g., Heiniö and Davies 2009; Cartigny et al. 2014). This, in turn, hampers the further applicability of the recent experimental progress in supercritical-flow regimes (Cartigny et al. 2014). The current study provides a 3D seismic anatomy of net-depositional cyclic steps in unconfined settings on the Bengal Fan and reconstructed the paleoflow parameters of turbidity currents involved in their construction. Our results, therefore, suggest that net-depositional cyclic steps are widespread, and contribute to a better understanding of 3d architectures of cyclic steps or long-wave, upstream-migrating bedforms.

Secondly, outcrop and core database show that cyclic steps are composed mainly of: (i) coarse-tail graded sediments with flame structures and homogenized substrate at hydraulic jumps (Lang and Winsemann 2013; Postma et al. 2014), (ii) poorly sorted, medium to very coarse, massive sandstones or alternating silt and fine-sand layers on their lee sides (Migeon et al. 2001; Ventra et al. 2015), and (iii) finer, better-sorted siltstones or sandstones on their stoss flanks (Ventra et al. 2015). Spatially, both core and seismic datasets of Normark et al. (2002) reveal that thicker and coarser beds preferentially deposited on their upcurrent flanks. However, plan-view distribution patterns of sandy supercritical-flow deposits in net-depositional cyclic steps remain undocumented, due to a lack of 3D anatomy of net-depositional cyclic steps. Ma et al. (2020) have suggested that high-amplitude events imaged as peak reflectors are seismic responses to low gamma *vs.* high resistivity well-log signatures away from the shale baseline, both of which are asymptomatic of sand-rich lithologies composed mainly of fine-grained sandstones and siltstones. High seismic amplitudes are high RMS attributes in the Bengal seismic database utilized in this study, therefore, represent seismic responses of sandy deposits. Characterizing these high amplitudes using RMS attribute-extraction maps above and below the hanging horizon of T_{wave} collectively reveals that sandy deposits coeval with the documented net-depositional cyclic steps in both fields 1 and 2 appear as high-RMS attribute accumulations that display closely spaced, long and linear, isolated, strike-elongated distribution patterns (Fig. 10). The proposed plan-view distribution patterns of sandy supercritical-flow deposits, therefore, have practical implications for predicting reservoir occurrence in supercritical-flow regimes.

9 Conclusions

3D seismic data and numerical computations of unconfined turbidity current conditions are used to investigate net-depositional cyclic steps in the Bay of Bengal, in terms of morphological properties, architectural styles, and flow dynamics.

Morphologically, the studied net-depositional cyclic steps have W of 587 to 2066 m (averaging 1375 m), H of 9 to 28 m (averaging 16 m), and W/H of 42 to 139 (averaging 87). They display asymmetrical cross-sections, which are composed of relatively steeper (β of 0.28° to 1.19°) and shorter (L_{lee} of 117 to 419 m) lee flanks and gentler (α of 0.16° to 0.18°) and longer (L_{stoss} of 410 to 1139 m) stoss sides, with bed pools (L_{jump} of 30 to 188 m) in between. Their lee sides

are 3 to 4 times steeper and 3 to 4 times shorter than their stoss sides.

Architecturally, the studied net-depositional cyclic steps occur in unconfined slope in the Bay of Bengal, are orthogonal to channel orientation, and are seen as strike-elongated, crescentic bedforms with straight to moderately sinuous crest lines. In a cross-sectional view, they are seismically imaged as rhythmically undulating, northward dipping, erosive, discontinuous reflections, and exhibit upstream-migrating growth patterns. Sandy supercritical-flow deposits coeval with Bengal net-depositional cyclic steps display closely spaced, long and linear, isolated, strike-elongated distribution patterns.

Hydrodynamically, unconfined turbidity currents were inferred to be involved in the construction of the Bengal net-depositional cyclic steps, based on their occurrence in unconfined settings, regular bifurcations, dispositional strike-parallel orientations of crest lines, and internal discontinuities. Unconfined turbidity currents on lee flanks of the documented cyclic steps had u of 2.70 to 3.98 m/s (averaging 3.24 m/s) and Fr of 1.53 to 2.27 (averaging 1.84), thereby displaying erosive, supercritical-flow regimes. Unconfined turbidity flows on their stoss flanks had u of 2.35 to 3.05 m/s (averaging 2.82 m/s) and Fr of 0.58 to 0.97 (averaging 0.84), thereby showing depositional, subcritical flow conditions. Bengal undulating bedforms were, thus, related to supercritical-to-subcritical flow transformations through internal hydraulic jumps, which gave rise to cyclic steps positive relative to the surrounding region of the seafloor, suggesting the predominant deposition of draping sediments associated with net-depositional cyclic steps.

Acknowledgements This research was jointly funded by PetroChina Hangzhou Research Institute of Geology (No. 2019D-4309). We acknowledge Chinnery Assets limited Company and Woodside for supporting research on this study and allowing publication.

References

Armitage DA, McHargue T, Fildani A, et al. Postavulsion channel evolution: Niger Delta continental slope. AAPG Bull. 2012;96(5):823–43. https://doi.org/10.1306/09131110189.

Bastia R, Das S, Radhakrishna M. Pre- and post-collisional depositional history in the upper and middle Bengal Fan and evaluation of deepwater reservoir potential along the northeast Continental Margin of India. Mar Pet Geol. 2010;27(9):2051–61. https://doi.org/10.1016/j.marpetgeo.2010.04.007.

Blum M, Rogers K, Gleason J, Najman Y, et al. Allogenic and autogenic signals in the stratigraphic record of the deep-sea Bengal Fan. Sci Rep. 2018;8(1):7973. https://doi.org/10.1038/s41598-018-25819-5.

Bowen AJ, Normark WR, Piper DJW. Modeling of turbidity currents on Navy submarine fan, California Continental Borderland. Sedimentology. 1984;31:169–85. https://doi.org/10.1002/9781444304473.ch1.

Cartigny MJB, Postma G, Van Den Berg JH, et al. A comparative study of sediment waves and cyclic steps based on geometries, internal structures and numerical modelling. Mar Geol. 2011;280(1–4):40–56. https://doi.org/10.1016/j.margeo.2010.11.006.

Cartigny MJB, Ventra D, Postma G, et al. Morphodynamics and sedimentary structures of bedforms under supercritical-flow conditions: new insights from flume experiments. Sedimentology. 2014;61(3):712–48. https://doi.org/10.1111/sed.12076.

Covault JA, Kostic S, Paull CK, et al. Submarine channel initiation, filling and maintenance from sea-floor geomorphology and morphodynamic modelling of cyclic steps. Sedimentology. 2014;61(4):1031–54. https://doi.org/10.1111/sed.12084.

Covault JA, Kostic S, Paull CK, et al. Cyclic steps and related supercritical bedforms: building blocks of deep-water depositional systems, western North America. Mar Geol. 2017;393:4–20. https://doi.org/10.1016/j.margeo.2016.12.009.

Curray JR. The Bengal Depositional System: from rift to orogeny. Mar Geol. 2014;352(2):59–69. https://doi.org/10.1016/j.margeo.2014.02.001.

Curray JR, Emmel FJ, Moore DG. The Bengal Fan: morphology, geometry, stratigraphy, history and processes. Mar Pet Geol. 2003;19(10):1191–223. https://doi.org/10.1016/S0264-8172(03)00035-7.

Dietrich P, Ghienne JF, Normandeau A, et al. Upslope-migrating bedforms in a proglacial sandur delta: cyclic steps from river-derived underflows? J Sediment Res. 2016;86(2):113–23. https://doi.org/10.2110/jsr.2016.4.

Ercilla G, Alonso B, Wynn RB, et al. Turbidity current sediment waves on irregular slopes: observations from the Orinoco sediment-wave field. Mar Geol. 2002;192(1–3):171–87. https://doi.org/10.1016/S0025-3227(02)00554-6.

Fildani A, Normark WR, Kostic S, et al. Channel formation by flow stripping: large-scale scour features along the Monterey East Channel and their relation to sediment waves. Sedimentology. 2006;53:1265–87. https://doi.org/10.1111/j.1365-3091.2006.00812.x.

Fournier L, Fauquembergue K, Zaragosi S, et al. The Bengal fan: external controls on the Holocene Active Channel turbidite activity. Holocene. 2016;27(6):900–13. https://doi.org/10.1177/0959683616675938.

Fricke AT, Sheets BA, Nittrouer CA, et al. An examination of Froude-supercritical flows and cyclic steps on a subaqueous lacustrine delta, Lake Chelan, Washington, USA. J Sediment Res. 2015;85(7):754–67. https://doi.org/10.2110/jsr.2015.48.

Gong CL, Wang YM, Peng XC, et al. Sediment waves on the South China Sea Slope off southwestern Taiwan: implications for the intrusion of the Northern Pacific Deep Water into the South China

Sea. Mar Pet Geol. 2012;32(1):95–109. https://doi.org/10.1016/j.marpetgeo.2011.12.005.
Gong CL, Chen LQ, Logan W. Asymmetrical, inversely graded, upstream-migrating cyclic steps in marine settings: late Miocene-early Pliocene Fish Creek-Vallecito Basin, southern California. Sediment Geol. 2017;360:35–46. https://doi.org/10.1016/j.sedgeo.2017.09.002.
Hand BM. Supercritical flow in density currents. J Sediment Pet. 1974;44(3):637–48. https://doi.org/10.1306/74D72AB3-2B21-11D7-8648000102C1865D.
Heiniö P, Davies RJ. Trails of depressions and sediment waves along submarine channels on the continental margin of Espirito Santo Basin, Brazil. Geol Soc Am Bull. 2009;121(5–6):698–711. https://doi.org/10.1130/B26190.1.
Hohbein M, Cartwright J. 3D seismic analysis of the West Shetland Drift system. Implications for Late Neogene palaeoceanography of the NE Atlantic. Mar Geol. 2006;230(1):1–20. https://doi.org/10.1016/j.margeo.2006.03.009.
Hughes Clarke JE. First wide-angle view of channelized turbidity currents links migrating cyclic steps to flow characteristics. Nat Commun. 2016;7:11896. https://doi.org/10.1038/ncomms11896.
Hughes Clarke JE, Videra Marques CR, Pratomo D. Imaging active mass-wasting and sediment flows on a fjord delta, Squamish, British Columbia. In: Krastel S, et al., editors. Submarine mass movements and their consequences VI: advances in natural and technological hazards research, vol. 37. 2014. p. 249–60. https://doi.org/10.1007/978-3-319-00972-8_22.
Komar PD. Hydraulic jumps in turbidity currents. GSA Bull. 1971;82(6):1477–87. https://doi.org/10.1130/0016-7606(1971)82%5b1477:HJITC%5d2.0.CO;2.
Kostic S. Modelling of submarine cyclic steps: controls on their formation, migration, and architecture. Geosphere. 2011;7(2):294–304. https://doi.org/10.1130/GES00601.1.
Kostic S. Upper flow regime bedforms on levees and continental slopes: turbidity current flow dynamics in response to fine-grained sediment waves. Geosphere. 2014;10(6):1094–103. https://doi.org/10.1130/GES01015.1.
Kostic S, Parker G. The response of turbidity currents to a canyon-fan transition: internal hydraulic jumps and depositional signatures. J Hydraul Res. 2006;44(5):631–53. https://doi.org/10.1080/00221686.2006.9521713.
Kostic S, Sequeiros O, Spinewine B, et al. Cyclic steps: a phenomenon of supercritical shallow flow from the high mountains to the bottom of the ocean. J Hydro-Environ Res. 2010;3(4):167–72. https://doi.org/10.1016/j.jher.2009.10.002.
Kottke B, Schwenk T, Breitzke M, et al. Acoustic facies and depositional processes in the upper submarine canyon swatch of no ground (Bay of Bengal). Deep-Sea Res II. 2003;50:979–1001. https://doi.org/10.1016/S0967-0645(02)00616-1.
Krishna KS, Bull JM, Scrutton RA. Early (pre-8 Ma) fault activity and temporal strain accumulation in the central Indian Ocean. GSA Bull. 2009;37(3):227–30. https://doi.org/10.1130/G25265A.1.
Kubo Y, Nakajima T. Laboratory experiments and numerical simulation of sediment–wave formation by turbidity currents. Mar Geol. 2002;192(1–3):105–21. https://doi.org/10.1016/S0025-3227(02)00551-0.
Lamb MP, Parsons JD, Mullenbach BL, et al. Evidence for superelevation, channel incision, and formation of cyclic steps by turbidity currents in Eel Canyon, California. GSA Bull. 2008;120(3):463–75. https://doi.org/10.1130/B26184.1.
Lang J, Winsemann J. Lateral and vertical facies relationships of bedforms deposited by aggrading supercritical flows: from cyclic steps to humpback dunes. Sediment Geol. 2013;296:36–54. https://doi.org/10.1016/j.sedgeo.2013.08.005.
Lang J, Brandes C, Winsemann J. Erosion and deposition by supercritical density flows during channel avulsion and backfilling: field examples from coarse-grained deepwater channel-levée complexes (Sandino Forearc Basin, southern Central America). Sediment Geol. 2017;349:79–102. https://doi.org/10.1016/j.sedgeo.2017.01.002.
Lee HJ, Syvitski JPM, Parker G, et al. Distinguishing sediment waves from slope failure deposits: field examples, including the 'Humboldt slide', and modelling results. Mar Geol. 2002;192(1–3):79–104. https://doi.org/10.1016/S0025-3227(02)00550-9.
Li L, Gong CL. Gradual transition from net erosional to net depositional cyclic steps along the submarine distributary channel thalweg in the Rio Muni Basin: a joint 3-D seismic and numerical approach. J Geophys Res Earth Surf. 2018;123(9):2087–106. https://doi.org/10.1029/2017JF004513.
Ma HX, Fan GZ, Shao DL, et al. Deep-water depositional architecture and sedimentary evolution in the Rakhine Basin, Northeast Bay of Bengal. Pet Sci. 2020;17:598–614. https://doi.org/10.1007/s12182-020-0042-0.
MacLachlan SE, Elliott GM, Parson LM. Investigations of the bottom current sculpted margin of Hatton Bank, NE Atlantic. Mar Geol. 2008;253(3–4):170–84. https://doi.org/10.1016/j.margeo.2008.05.012.
Masson DG, Howe JA, Stoker MS. Bottom-current sediment waves, sediment drifts and contourites in the northern Rockall Trough. Mar Geol. 2002;192(1):215–37. https://doi.org/10.1016/S0025-3227(02)00556-X.
Michels KH, Suckow A, Breitzke M, et al. Sediment transport processes in the shelf canyon 'Swatch of no Ground' (Bay of Bengal). Deep-Sea Res II. 2003;50:1003–22. https://doi.org/10.1016/S0967-0645(02)00617-3.
Migeon S, Savoyea B, Faugères JC. Quaternary development of migrating sediment waves in the Var deep-sea fan: distribution, growth pattern, and implication for levee evolution. Sediment Geol. 2000;133(3–4):265–93. https://doi.org/10.1016/s0037-0738(00)00043-9.
Migeon S, Savoye B, Zanella E, et al. Detailed seismic-reflection and sedimentary study of turbidite sediment waves on the Var Sedimentary Ridge (SE France): significance for sediment transport and deposition and for the mechanisms of sediment-wave construction. Mar Pet Geol. 2001;18(2):179–208. https://doi.org/10.1016/S0264-8172(00)00060-X.
Normandeau A, Lajeunesse P, Poiré AG, et al. Morphological expression of bedforms formed by supercritical sediment density flows on four fjord-lake deltas of the southeastern Canadian Shield (Eastern Canada). Sedimentology. 2016;63(7):2106–29. https://doi.org/10.1111/sed.12298.
Normark WR, Hess GR, Stow DAV, et al. Sediment waves on the Monterey Fan Levee: a preliminary physical interpretation. Mar Geol. 1980;37(1–2):1–18. https://doi.org/10.1016/0025-3227(80)90009-2.
Normark WR, Piper DJW, Posamentier H, et al. Variability in form and growth of sediment waves on turbidite channel levees. Mar Geol. 2002;192(1–3):23–58. https://doi.org/10.1016/S0025-3227(02)00548-0.
Parker G, Izumi N. Purely erosional cyclic and solitary steps created by flow over a cohesive bed. J Fluid Mech. 2000;419:203–38. https://doi.org/10.1017/S0022112000001403.
Paul H, Gaillot G, Strom K, et al. Linking hydraulic properties in supercritical submarine distributary channels to depositional-lobe geometry. J Sediment Res. 2017;87(9):935–50. https://doi.org/10.2110/jsr.2017.53.
Paull CK, Ussler WIII, Caress DW, et al. Origins of large crescent-shaped bedforms within the axial channel of Monterey Canyon, offshore California. Geosphere. 2010;6(6):755–74. https://doi.org/10.1130/GES00527.1.

Pickering KT, Corregidor J, Clark JD. Architecture and stacking patterns of lower slope and proximal basin-floor channelised submarine fans, Middle Eocene Ainsa System, Spanish Pyrenees: an integrated outcrop–subsurface study. Earth-Sci Rev. 2015;144:47–81. https://doi.org/10.1016/j.earscirev.2014.11.017.

Piper DJW, Savoye B. Processes of late Quaternary turbidity current flow and deposition on the Var deap-sea fan, north-west Mediterranean Sea. Sedimentology. 1993;40:557–82. https://doi.org/10.1111/j.1365-3091.1993.tb01350.x.

Pomar L, Morsilli M, Hallock P, et al. Internal waves, an underexplored source of turbulence events in the sedimentary record. Earth-Sci Rev. 2012;111(1–2):56–81. https://doi.org/10.1016/j.earscirev.2011.12.005.

Ponce JJ, Carmona N. Coarse-grained sediment waves in hyperpycnal clinoform systems, Miocene of the Austral foreland basin, Argentina. Geology. 2011;39(8):763–6. https://doi.org/10.1130/G31939.1.

Posamentier HW, Kolla V. Seismic geomorphology and stratigraphy of depositional elements in deep-water settings. J Sediment Res. 2003;73(3):367–88. https://doi.org/10.1306/111302730367.

Postma G, Cartigny MJB. Supercritical and subcritical turbidity currents and their deposits—a synthesis. Geology. 2014;42(11):987–90. https://doi.org/10.1130/G35957.1.

Postma G, Kleverlaan K, Cartigny MJB. Recognition of cyclic steps in sandy and gravelly turbidite sequences, and consequences for the Bouma facies model. Sedimentology. 2014;61(7):2268–90. https://doi.org/10.1111/sed.12135.

Schwenk T, Spieß V, Breitzke C, et al. The architecture and evolution of the Middle Bengal Fan in vicinity of the active channel-levee system imaged by high-resolution seismic data. Mar Pet Geol. 2005;22(5):637–56. https://doi.org/10.1016/j.marpetgeo.2005.01.007.

Sequeiros OE. Estimating turbidity current conditions from channel morphology: a Froude number approach. J Geophys Res. 2012;117:C04003. https://doi.org/10.1029/2011JC007201.

Slootman A, Cartigny JM. Cyclic steps: review and aggradation-based classification. Earth-Sci Rev. 2019;201:102949. https://doi.org/10.1016/j.earscirev.2019.102949.

Smith DP, Kvitek R, Iampietro PJ, et al. Twenty-nine months of geomorphic change in upper Monterey Canyon (2002–2005). Mar Geol. 2007;236(1):79–94. https://doi.org/10.1016/j.margeo.2006.09.024.

Sun T, Parker G. Transportational cyclic steps created by flow over an erodible bed: part 2. Theory and numerical simulation. J Hydraul Res. 2005;43(5):502–14. https://doi.org/10.1080/00221680509500148.

Symons WO, Sumner EJ, Talling PJ, et al. Large-scale sediment waves and scours on the modern seafloor and their implications for the prevalence of supercritical flows. Mar Geol. 2016;371:130–48. https://doi.org/10.1016/j.margeo.2015.11.009.

Taki K, Parker G. Transportational cyclic steps created by flow over an erodible bed: part 1. Experiments. J Hydraul Res. 2005;43(5):488–501. https://doi.org/10.1080/00221680509500147.

Talling PJ, Allin J, Armitage DA, et al. Key future directions for research on turbidity currents and their deposits. J Sediment Res. 2015;85(2):153–69. https://doi.org/10.2110/jsr.2015.03.

Vail R, Mitchum RM, Thompson S. Seismic stratigraphy and global changes of sea level, part 3: relative changes of sea level from coastal onlap. In: Payton CE (eds) Seismic stratigraphy applications to hydrocarbon exploration. AAPG Memoir. 1977;26:63–82.

Vellinga AJ, Cartigny MJ, Eggenhuisen JT, et al. Morphodynamics and depositional signature of low-aggradation cyclic steps: new insights from a depth resolved numerical model. Sedimentology. 2018;65:540–60. https://doi.org/10.1111/sed.12391.

Ventra D, Cartigny MJB, Bijkerk JF, et al. Supercritical-flow structures on a Late Carboniferous delta front: sedimentologic and paleoclimatic significance. Geology. 2015;43(12):731–4. https://doi.org/10.1130/G37231C.1.

Weber ME, Wiedicke-Hombach M, Kudrass HR, et al. Active growth of the Bengal Fan during sea-level rise and highstand. Geology. 1997;25(4):315–8. https://doi.org/10.1130/0091-7613(1997)025%3c0315:AGOTBF%3e2.3.CO;2.

Wynn RB, Stow DAV. Classification and characterization of deepwater sediment waves. Mar Geol. 2002;192(1–3):7–22. https://doi.org/10.1016/S0025-3227(02)00547-9.

Wynn RB, Weaver PPE, Ercilla G, et al. Sedimentary processes in the selvage sediment-wave field, NE Atlantic: new insights into the formation of sediment waves by turbidity currents. Sedimentology. 2000a;47(6):1181–97. https://doi.org/10.1046/j.1365-3091.2000.00348.x.

Wynn RB, Masson DG, Stow DAV, et al. Turbidity current sediment waves on the submarine slopes of the western Canary Islands. Mar Geol. 2000b;163(1–4):185–98. https://doi.org/10.1016/S0025-3227(99)00101-2.

Xu JP, Wong FL, Kvitek R, et al. Sandwave migration in Monterey Submarine Canyon, Central California. Mar Geol. 2008;248(3–4):193–212. https://doi.org/10.1016/j.margeo.2007.11.005.

Yang SY, Kim JW. Pliocene basin-floor fan sedimentation in the Bay of Bengal (offshore northwest Myanmar). Mar Pet Geol. 2014;49:45–58. https://doi.org/10.1016/j.marpetgeo.2013.09.007.

Yin A. Cenozoic tectonic evolution of the Himalayan orogen as constrained by along-strike variation of structural geometry, exhumation history, and foreland sedimentation. Earth-Sci Rev. 2006;76(1–2):1–131. https://doi.org/10.1016/j.earscirev.2005.05.004.

Zhan LF, Guo BC, Yu YJ. Architectural elements and stratigraphy of a deepwater fan: a case study of the Bengal Fan, Rakhine Basin, offshore Myanmar. Arab J Geosci. 2019;12:212. https://doi.org/10.1007/s12517-019-4378-0.

Zhong GF, Cartigny MJB, Kuang ZG, et al. Cyclic steps along the South Taiwan Shoal and West Penghu submarine canyons on the northeastern continental slope of the South China Sea. GSA Bull. 2015;127(5–6):804–24. https://doi.org/10.1130/B31003.